JOURNAL OF PROPULSION AND POWER
Vol. 22, No. 5, September–October 2006

Thermal Decomposition of Hydrogen Peroxide, Part 2: Modeling Studies

J. H. Corpening,* S. D. Heister,† and W. E. Anderson‡
Purdue University, West Lafayette, Indiana 47906
and
B. J. Austin§
InSpace, LLC., West Lafayette, Indiana 47906

A one-dimensional model has been developed to investigate the thermal decomposition of high-concentration hydrogen peroxide (HP) in a stream of previously decomposed HP products. The model developed assumes steady, one-dimensional adiabatic flow and includes basic mass balances, droplet evaporation, gas-phase decomposition kinetics, droplet dynamics, and control volume conservation laws. The model accounts for various HP concentration levels for both main and secondary flows, mass flow rates for both flows, and initial temperature of each. Results are shown to be consistent with prior experimental measurements. Parametric studies are presented to assess the effects of initial droplet size, secondary injectant flow, mass velocity in the primary stream, peroxide concentration, and initial liquid temperature on the decomposition process. In general, results indicate unacceptably long decomposition distances assuming 90% HP decomposition products in the primary stream. Using 98% HP showed some improvement due to the enhanced decomposition temperature of this fluid as compared to 90% HP.

Nomenclature

A	=	duct cross-sectional area, m^2
A_0	=	frequency factor, s^{-1}
C	=	concentration
C_P	=	specific heat, J/kg · K
D	=	drop diameter, μm
E_a	=	activation energy, J/mol
h_{rxn}	=	heat of reaction, J/kg
K	=	unimolecular rate, s^{-1}
k	=	thermal conductivity, W/m · K
m_g	=	total gas mass in control volume, kg
$\dot{m}$	=	mass flow, kg/s
n	=	number of droplets
P	=	pressure, Pa
R_u	=	universal gas constant, J/mol · K
r	=	ratio of secondary to primary
T	=	temperature of mix, K
t	=	time, s
v	=	velocity, m/s
W	=	molecular weight, g/gmol
x	=	axial distance, m
y	=	mass fraction
η	=	efficiency
ρ	=	density, kg/m^3

Subscripts

cat	=	catalyst
CV	=	control volume
drop	=	droplet
evap	=	evaporation
HP	=	hydrogen peroxide
kin	=	kinetics
liq	=	liquid
mix	=	mixture
oxy	=	oxygen
p	=	products
r	=	reacted
s	=	secondary
sat	=	saturation
vap	=	vapor
wat	=	water
0	=	initial

Received 7 September 2004; revision received 21 April 2005; accepted for publication 18 May 2005.

*Graduate Student, School of Aeronautics and Astronautics.
†Professor, School of Aeronautics and Astronautics. Associate Fellow AIAA.
‡Assistant Professor, School of Aeronautics and Astronautics. Member AIAA.
§General Manager and P.I. Member AIAA.

Introduction

HIGH-CONCENTRATION hydrogen peroxide has received increased attention for storable oxidizer applications in recent years due to its relative ease of use and low toxicity. The monopropellant characteristics of this fluid also provide unique advantages in many applications and permit the use of decomposition products for power generation or for use in staged bipropellant systems. Catalyst beds using silver screens or other catalytic material are frequently utilized to initiate decomposition of the fluid. However, the catalyst beds become quite bulky in higher mass flow applications, and there is an interest in a separate injection of liquid peroxide downstream of a catalyst bed exhaust to minimize system mass. In this concept, the aft-injected liquid would undergo evaporation and thermal decomposition of the hydrogen peroxide vapor evolved in this process. The focus of the present study is to develop a one-dimensional model that, through theory and experiment,[1] permits analysis of this process under arbitrary injection and catalyst bed exhaust conditions. In the companion paper to this work,[1] an extensive review of the prior work is undertaken, and in the interest of brevity, this discussion will not be repeated here. The following section provides a description of the model elements; results are then provided for a variety of flow conditions.

Model Development

We presume a steady, one-dimensional adiabatic flow for the purposes of the study. Figure 1 introduces some of the relevant variables in the problem; the remainder are defined in the nomenclature

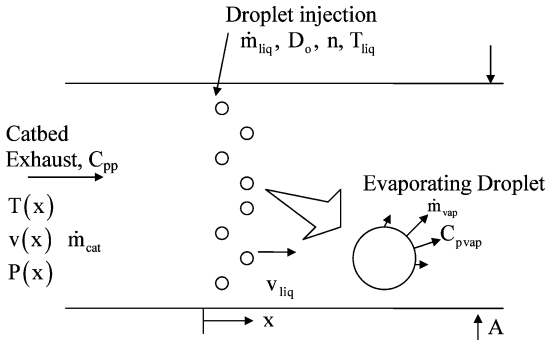

Fig. 1 Definitions of variables/nomenclature associated with model.

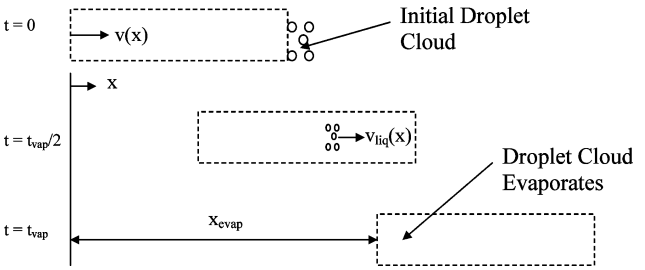

Fig. 2 Control volume of gas (dashed lines) combined with given packet of liquid droplets over time interval t_v.

section. Wall friction is neglected because the Reynolds numbers in problems of interest are very large. The aft-injected liquid spray is assumed to be monodisperse with a droplet size corresponding to its Sauter mean diameter (the equivalent diameter providing the correct total surface area in the spray). The gas-phase composition is permitted to evolve in time, and changes are reflected by vaporized and thermally decomposed hydrogen peroxide. The specific heats of the decomposition products and of the hydrogen peroxide vapor are presumed to be constant in the analysis. The decomposition reaction is assumed to obey first-order unimolecular reaction kinetics per the work of prior researchers.[2–8] Major model elements include basic mass balances, kinetics modeling, droplet dynamics, and control volume conservation laws. These elements are discussed in the following subsections.

Mass Balances

The relative slip between the phases creates significant issues in the analysis. Presume that at $t = 0$ we begin with a collection of n droplets of initial diameter D_0. These droplets are accelerated and evaporated by the gas stream over a time t_{vap}. The gases passing over the droplet cloud are assumed to be initially at the freestream conditions defined by the catalyst bed exhaust, and the vapor emanating from the drops is presumed to be convected downstream at the velocity of the mixture. The distance traveled by the gas stream, x_{evap}, during this evaporation time can be estimated assuming constant gas velocity,

$$x_{evap} = v_{cat\_0} t_{vap} \tag{1}$$

A control volume can be defined that includes the n_d droplets and the volume and mass of catalyst bed gases that interact with the droplet cloud during the time which it is evaporating. Figure 2 provides a schematic of this control volume with an assumed constant cross-sectional area A. As shown in Fig. 2, the gas travels distance x_{vg} during the evaporation time. The mass of catalyst bed exhaust that interacts with the evaporating cloud can be expressed as

$$m_{cat} = \dot{m}_{cat} t_{vap} \tag{2}$$

Assuming a quasi-steady process with regard to the injection and bulk inflow of gases, the flow rate ratio between the liquid injectant and gas must be the same as the mass ratio in the selected control volume. Under this constraint, we may write

$$\frac{m_{drop}}{m_{cat}} = \frac{\dot{m}_{liq}}{\dot{m}_{cat}} = \frac{n \rho_{liq} \pi D_0^3}{6 m_{cat}} \tag{3}$$

such that the number of droplets required to achieve the given flow split is then

$$n = \frac{6 \dot{m}_{liq} t_{vap}}{\pi \rho_{liq} D_0^3} \tag{4}$$

As the droplets evaporate, they will change the composition and mass of gas within the control volume. There will be a stratification of gas composition, pressure, and temperature as a result of the mixing of the vapor and the catalyst bed exhaust and from any decomposition reactions that occur during the time when the drops are evaporating. Droplets on the upwind side of the cloud will be immersed in catalyst bed exhaust conditions, whereas drops on the downstream side of the cloud will be immersed in cooled gases of different composition as a result of mixing of evaporant with the catalyst bed gases. To address this stratification issue, a Lagrangian approach is used to track the mean properties of the cloud presuming that the vaporization rate is controlled by the energy interchange with the bulk temperature/composition of the gases (both catalyst bed and evaporant) within the control volume. In this manner, the local gas composition is coupled to the droplet properties and evaporation rate. Using this approach, we begin by computing the average initial composition of the gases in the control volume. Assuming that 90% hydrogen peroxide is decomposed in the catalyst bed the decomposition reaction for this concentration can be written as

$$H_2O_2 + 0.210 H_2O \rightarrow 1.210 H_2O + \tfrac{1}{2} O_2$$

so that the initial mass of water and oxygen present in the control volume may be expressed as

$$m_{wat\_0} = 0.424\, m_{cat}, \qquad m_{oxy\_0} = 0.576\, m_{cat} \tag{5}$$

Water is created via thermal decomposition of hydrogen peroxide (HP) vapor and from the portion of water evaporated from the 90% fluid assumed to be injected into the chamber. The resultant water flow can be expressed as

$$\dot{m}_{wat} = 0.1\, \dot{m}_{vap} - (18/34)\, \dot{m}_r \tag{6}$$

where $\dot{m}_r$ is the rate of thermal decomposition reactions within the evaporated peroxide gas. (Note that $\dot{m}_r$ will be a negative number in that the reactions decrease the amount of HP vapor in the control volume.) Similarly, the rate at which oxygen is created from the thermal decomposition reaction can be expressed as

$$\dot{m}_{oxy} = (-16/34)\, \dot{m}_r \tag{7}$$

Finally, the rate of net peroxide vapor generation (assuming 90% HP in the drops) is

$$\dot{m}_{HP} = 0.9\, \dot{m}_{vap} + \dot{m}_r \tag{8}$$

where vaporization increases peroxide content and the decomposition reaction destroys HP in the control volume. Here we have assumed that the droplet evaporates uniformly in the sense that water is driven off at the equilibrium composition (10% of the droplet mass). In actuality, water is evaporated preferentially, at least to some extent during the vaporization process. Because the vaporization process happens quickly in the cases of interest, we neglect this effect. Equations (6–8) can be integrated in time subject to the initial conditions given in Eq. (4) and the fact that $m_{HP\_0} = 0$, that is, drops begin to evaporate at $t = 0$. The vaporization and thermal decomposition rates appearing in Eqs. (6–8) are discussed in a subsequent section. Equations (6–8) are integrated using Huen's method, which is a second-order scheme based on trapezoidal integration (see Ref. 9).

When the results of the mass integrations are used, the total gas mass in the control volume at any instant in time can be expressed as

$$m_g = m_{\text{wat}} + m_{\text{oxy}} + m_{\text{HP}} \tag{9}$$

and the instantaneous mass fractions (gas phase only) of the constituents can be computed,

$$y_{\text{wat}} = m_{\text{wat}}/m_g \qquad y_{\text{oxy}} = m_{\text{oxy}}/m_g \qquad y_{\text{HP}} = m_{\text{HP}}/m_g \tag{10}$$

Finally, the resultant molecular weight of the mixture W_{mix} can be expressed in terms of the mass fractions and individual constituent molecular weights

$$W_{\text{mix}}(x) = [1/(y_{\text{wat}}/W_{\text{wat}})] + [1/(y_{\text{oxy}}/W_{\text{oxy}})] + [1/(y_{\text{HP}}/W_{\text{HP}})] \tag{11}$$

Kinetics Model

The concentration of HP, C_{HP}, can be related to the mass fraction of HP present in the gases within the control volume,[10]

$$C_{\text{HP}} = y_{\text{HP}} \frac{P W_{\text{mix}}}{R_u T W_{\text{HP}}} \tag{12}$$

The unimolecular kinetics reaction can be written as

$$\frac{\mathrm{d}C_{\text{HP}}}{\mathrm{d}t} = -K C_{\text{HP}} \tag{13}$$

where $K = A_0 \exp(-Ea/RuT) = K(x)$ in the present problem. Data from the literature provide the following for the frequency factor and activation energy[3,4]:

$$A_0 = 10^{13}/\text{s} \qquad E_a = 200{,}864.6 \text{ J/mol}$$

In Ref. 11 a summary of previous kinetics studies is provided. Combining Eqs. (12) and (13) provides an expression for the concentration or mass fraction of HP,

$$C_{\text{HP}}\left(\frac{1}{y_{\text{HP}}}\frac{\mathrm{d}y_{\text{HP}}}{\mathrm{d}t} + \frac{v}{P}\frac{\mathrm{d}P}{\mathrm{d}x} + \frac{1}{W_{\text{mix}}}\frac{\mathrm{d}W_{\text{mix}}}{\mathrm{d}t} - \frac{v}{T}\frac{\mathrm{d}T}{\mathrm{d}x}\right) = -K C_{\text{HP}}$$

or

$$\frac{\mathrm{d}y_{\text{HP}}}{\mathrm{d}t} = y_{\text{HP}}\left(-K - \frac{v}{P}\frac{\mathrm{d}P}{\mathrm{d}x} - \frac{1}{W_{\text{mix}}}\frac{\mathrm{d}W_{\text{mix}}}{\mathrm{d}t} + \frac{v}{T}\frac{\mathrm{d}T}{\mathrm{d}x}\right) \tag{14}$$

Here, we have transformed time derivatives to spatial derivatives for the pressure and temperature terms in Eq. (14) in accordance with the steady-state hypothesis. These fluid properties are assumed to correspond to bulk properties in the control volume, and conservation of momentum and energy will ultimately be used to compute these terms (as shown in the following section). Because the fluid in the control volume is assumed to travel at the bulk gas velocity v, the time increment is related to the spatial increment via $\mathrm{d}t = \mathrm{d}x/v$. Now, the mole fraction of hydrogen peroxide can be related to the mass of hydrogen peroxide and total mass in the control volume, $y_{\text{HP}} = m_{\text{HP}}/m_{\text{CV}}$, such that

$$\frac{\mathrm{d}y_{\text{HP}}}{\mathrm{d}t} = y_{\text{HP}}\left(\frac{\dot{m}_{\text{HP}}}{m_{\text{CV}}} - \frac{\dot{m}_{\text{CV}}}{m_{\text{CV}}}\right) \tag{15}$$

Thus, inserting Eq. (15) into Eq. (14) provides the rate of HP mass change with time due to decomposition reactions within the control volume,

$$\left.\frac{\mathrm{d}m_{\text{HP}}}{\mathrm{d}t}\right)_{\text{kin}} = \frac{\mathrm{d}m_r}{\mathrm{d}t} = m_{\text{HP}}\left[\frac{1}{m_{\text{CV}}}\frac{\mathrm{d}m_{\text{CV}}}{\mathrm{d}t} - K - \frac{v}{P}\frac{\mathrm{d}P}{\mathrm{d}x} - \frac{1}{W_{\text{mix}}}\frac{\mathrm{d}W_{\text{mix}}}{\mathrm{d}t} + \frac{v}{T}\frac{\mathrm{d}T}{\mathrm{d}x}\right] \tag{16}$$

Equation (16) describes the rate of gas decomposition due solely to kinetics effects. In our problem, we also have mass addition of HP vapor due to droplet vaporization (when drops are present). For a 90% peroxide drop undergoing nonpreferential vaporization, $\mathrm{d}\dot{m}_{\text{HP}} = 0.9\,\mathrm{d}\dot{m}_v$. We need to add this contribution to offset decreases in peroxide vapor flow due to decomposition. Adding this contribution to Eq. (16) we obtain

$$\frac{\mathrm{d}m_{\text{HP}}}{\mathrm{d}t} = m_{\text{HP}}\left[\frac{1}{m_{\text{CV}}}\frac{\mathrm{d}m_{\text{CV}}}{\mathrm{d}t} - K - \frac{v}{P}\frac{\mathrm{d}P}{\mathrm{d}x} - \frac{1}{W_{\text{mix}}}\frac{\mathrm{d}W_{\text{mix}}}{\mathrm{d}t} + \frac{v}{T}\frac{\mathrm{d}T}{\mathrm{d}x}\right] + 0.9\,\dot{m}_{\text{vap}} \tag{17}$$

Droplet Evaporation and Dynamics Model

The mass addition from vaporization can be computed using the simplified D^2 law model,[10]

$$\dot{m}_{\text{vap}} = 2\pi\left(\frac{k_{\text{liq}} D}{C_{p\text{vap}}}\right)\ell_n(1 + B_q) \tag{18}$$

where the k_{liq} is liquid thermal conductivity and Spalding number B_q is defined as

$$B_q = C_{p\text{vap}}\frac{(T - T_{\text{sat}})}{[h_v + C_{p\text{liq}}(T_{\text{sat}} - T_{\text{liq}})]} \tag{19}$$

This parameter measures the ratio of the enthalpy driving the evaporation to the enthalpy required to evaporate the fluid in the drop. Because the gas temperature varies with time/space in this application, Eq. (18) must be integrated numerically and the droplet size history does not exactly correspond to a D^2 law behavior.

Considering the forces on an individual drop, we can determine its instantaneous acceleration,

$$\frac{\mathrm{d}v_{\text{liq}}}{\mathrm{d}t} = \frac{A_{\text{drop}} C_D \rho (v - v_{\text{liq}})^2}{2 m_{\text{drop}}} \tag{20}$$

where C_D is the drag coefficient, A_{drop} is the projected area, and the mass of drop m_{drop} is computed from the mass lost from vaporization at any instant in time,

$$m_{\text{drop}} = m_{\text{drop\_0}} - \int_{t=0}^{t} \dot{m}_{\text{vap}}\,\mathrm{d}t \tag{21}$$

The instantaneous droplet diameter and cross-sectional area are computed assuming the drop remains spherical,

$$D = \sqrt[3]{6 m_{\text{drop}}/\pi\rho_{\text{liq}}}, \qquad A_{\text{drop}} = (\pi/4)[D(t)]^2 \tag{22}$$

As the droplet becomes vanishingly small, several of the earlier given drop characteristic equations tend to diverge. For this reason, we choose a practical lower limit on the droplet mass to avoid numerical difficulties in integrating the equations beyond the point where drops vanish. Droplets are assumed to be completely vaporized when their mass is reduced to 0.1% of the initial droplet mass. This threshold provides adequate accuracy in mass, energy, and momentum balances on the control volume.

Control Volume Conservation Laws

As already mentioned, the control volume for the analysis is assumed to be the mass of gas that passes over a given packet of droplets. The size of the control volume is fundamentally set by the droplet vaporization time as noted in Eqs. (1–4). The properties of the gas within the two-phase mixture are computed assuming perfect mixing of all evaporated peroxide/water with the remaining gases within the control volume. This assumption allows one to compute the bulk properties of the mixture as a function of distance traveled by the gas. Furthermore, the average environment realized by droplets within the control volume is assumed to be represented by gas properties computed under this assumption as already stated in

the earlier droplet dynamics discussion. The momentum and energy balances on the control volume follow the approach of Shapiro and Moran.[12] The unsteady evolution of the two-phase flow is treated in a parabolic fashion wherein gas property changes are determined by a spatial stepping procedure along the length of the combustion chamber.

Energy interactions occur with the droplets via the opposing interactions of energy lost to vaporize the drops and energy gained from thermal decomposition. Kinetic energy interactions are small in the subsonic flows of interest, but are maintained for completeness. The initial thermal and kinetic energy entering an incremental control volume can be expressed as

$$(m_{\text{wat}} + m_{\text{oxy}})C_{pp}T + m_{\text{HP}}C_{p\text{vap}}T + 0.5m_{\text{vap}}^2 \tag{23}$$

Here m is the gas mixture mass and C_{pp} and $C_{p\text{vap}}$ are constant pressure specific heats of the decomposition products and HP vapor, respectively. The energy leaving the incremental control volume includes changes due to mass additions from vaporization, temperature changes, energy contributed to evaporated liquid, and energy liberated from the decomposition of HP vapor,

$$\begin{aligned}&(m_{\text{wat}} + \mathrm{d}m_{\text{wat}} + m_{\text{oxy}} + \mathrm{d}m_{\text{oxy}})C_{pp}(T + \mathrm{d}T)\\ &\quad + (m_{\text{HP}} + \mathrm{d}m_{\text{HP}})C_{p\text{vap}}(T + \mathrm{d}T) + 0.5(m + \mathrm{d}m)(v + \mathrm{d}v)^2\\ &\quad + \mathrm{d}m_{\text{vap}}h_{lv} + \mathrm{d}m_r h_{rxn}\end{aligned} \tag{24}$$

where h_{lv} measures the energy required to heat the evaporated liquid to its saturation temperature, to vaporize it, and to superheat it to the local mixture temperature,

$$h_{lv} = C_{p\text{vap}}(T - T_{\text{sat}}) + h_{\text{vap}} + C_{p\text{liq}}(T_{\text{sat}} - T_{\text{liq}}) \tag{25}$$

T_{sat} is the saturation temperature of the 90% HP, h_{vap} is the heat of vaporization, and T_{liq} is the liquid temperature at which the drops are injected. Equating Eqs. (23) and (24) and dividing both sides by the time increment $\mathrm{d}t$ provides the final form for the energy balance,

$$\frac{\mathrm{d}T}{\mathrm{d}t} = \frac{1}{mC_p}\left\{\begin{aligned}&-\dot{m}_r h_{rxn} - [(\dot{m}_{\text{wat}} + \dot{m}_{\text{oxy}})C_{pp} + \dot{m}_{\text{HP}}C_{p\text{vap}}]T \cdots\\ &\cdots - \dot{m}_{\text{vap}}h_{lv} - mv\frac{\mathrm{d}v}{\mathrm{d}t} - \dot{m}\frac{v^2}{2}\end{aligned}\right\} \tag{26}$$

where $mC_p = (m_{\text{wat}} + m_{\text{oxy}})C_{pp} + m_{\text{HP}}C_{p\text{vap}}$. Initially, the temperature is set to the temperature of the catalyst bed exhaust to provide the condition for initiating integration of Eq. (26).

The gas pressure distribution in the combustion chamber can be determined from a momentum balance on the control volume. Pressure forces and drag on the droplets represent the two forces imposed on the fluid, and momentum interactions also occur due to the mass addition from the vaporized fluid. The relevant differential form of the momentum equation can be expressed as

$$PA - (P + \mathrm{d}P)A - \mathrm{d}X = (\dot{m} + \mathrm{d}\dot{m}_{\text{vap}})(v + \mathrm{d}v) - \dot{m}v - v_{\text{liq}}\,\mathrm{d}\dot{m}_{\text{vap}}$$

or

$$-A\,\mathrm{d}P = \mathrm{d}X + \dot{m}\,\mathrm{d}v + v\,\mathrm{d}\dot{m} - v_{\text{liq}}\,\mathrm{d}\dot{m}_{\text{vap}} \tag{27}$$

Here, the flow rate changes are entirely attributable to vaporization such that $\mathrm{d}\dot{m} = \mathrm{d}\dot{m}_{\text{vap}}$. The net drag force on the droplet may be expressed as

$$X = C_D\tfrac{1}{2}\rho(v - v_{\text{liq}})^2(\pi/4)D^2 \tag{28}$$

Substituting Eq. (28) into Eq. (27), we obtain

$$\frac{\mathrm{d}P}{\mathrm{d}x} = -\frac{1}{A}\frac{\mathrm{d}X}{\mathrm{d}x} - \frac{\dot{m}}{A}\frac{\mathrm{d}v}{\mathrm{d}x} - \frac{(v - v_{\text{liq}})}{A}\frac{\mathrm{d}\dot{m}_r}{\mathrm{d}x} \tag{29}$$

When the fact that $v = \mathrm{d}x/\mathrm{d}t$ is used, the derivative $\mathrm{d}\dot{m}_r/\mathrm{d}x = v\,\mathrm{d}\dot{m}_r/\mathrm{d}t$. The remaining derivatives on the right-hand side of Eq. (29) are determined from first-order upwind differencing. The initial pressure is an input to the model, and the drops are assumed to enter with no axial component of velocity in computing their initial drag.

Table 1 Constant HP properties used

Property	Value	Unit
Liquid specific heat C_{pl}	2774	J/kg · K
Molecular weight, 90% HP	31.3	g/g · mol
Saturation temperature T_{sat}	414.5	K
Binary diffusivity	$3.35e^{-8}$	m^2/s
Activation energy E_a	200,865	J/mol
Rate constant A_0	10^{13}	s^{-1}
Vapor thermal conductivity	0.0938	W/m · K

The gas density ρ is computed from the perfect gas law,

$$\rho = PW_{\text{mix}}/R_u T \tag{30}$$

and the local gas velocity is computed from the continuity equation

$$v = \dot{m}/\rho A \tag{31}$$

where A is the cross-sectional area of the combustion chamber.

Gas and Liquid Thermodynamic Properties

All gas and liquid thermodynamic properties for HP were taken from Ref. 13. For the viscosity, liquid thermal conductivity, density, and vapor specific heat, fourth-order curve fits were calculated from graphical data. Also, a specific curve fit was provided for the vapor pressure of 90% HP. Other parameters such as liquid specific heat, molecular weight, saturation temperature, binary diffusivity, activation energy, rate constant, and vapor thermal conductivity were taken as constant values over the entire decomposition process. All values used are listed in Table 1.

Solution Methodology

Time and spatial integrations are performed using a second-order trapezoidal integration scheme, Huen's method, as already mentioned. The solution methodology for the scheme is as follows.

1) Input initial conditions including chamber diameter, catalyst bed flow rate, pressure, temperature, secondary liquid injection flow rate, droplet size, and known constants related to thermodynamic and kinetic properties of the mixture.

2) Input or guess a vaporization time t_v.

3) Compute the number of droplets, initial catalyst bed gas, liquid, oxygen, and water vapor masses per Eqs. (2–5).

4) Compute/input the desired time step and initialize the time to $t = 0$.

5) Begin the time stepping loop.

6) Compute current values of derivatives of control volume masses [Eqs. (6–8)], reacted and vaporized masses [Eqs. (16) and (17)], droplet temperature and velocity [Eqs. (18) and (20)], droplet mass and diameter [Eqs. (21) and (22)], gas temperature [Eq. (26)] and pressure [Eq. (29)], and current gas density and velocity [Eqs. (30) and (31)].

7) Compute predicted values at the new time level using Huen's method. For the equation $\mathrm{d}y/\mathrm{d}t = f(x)$, we would define the predicted value at the new time level as $y^* = y_i + \Delta t(\mathrm{d}y/\mathrm{d}t)|_i$, where the subscript i denotes the current time level and Δt denotes the time step. Predicted values are computed for all dependent variables including masses, mass fractions, gas conditions, droplet size and mass, liquid temperature, gas and liquid properties at the new predicted temperature and pressure, gas and liquid velocities, and droplet drag.

8) Compute derivatives described in step 6 at the new time level using the starred quantities computed in step 7. For example, we define $(\mathrm{d}y/\mathrm{d}t)^* = f(x^*)$, where x^* is the dependent variable as computed in step 7. The $\mathrm{d}y/\mathrm{d}t^*$ value is the predicted slope of the function at the new time level.

9) Take a time step $(t = t + \Delta t)$ and compute updated values for all dependent variables using Huen's method: $y_{i+1} = y_i + 0.5\Delta t(\mathrm{d}t/\mathrm{d}t|_i + \mathrm{d}y/\mathrm{d}t^*)$. With use of this approach,

update gas mass and composition, droplet mass, gas-phase properties, liquid temperature, and droplet size. If the droplet mass falls below the selected threshold value (0.1% of its initial mass), set a flag to eliminate computations involving droplets and set the droplet size to zero. Record the vaporization time t_v coincident with this event.

10) Return to step 5 until the desired number of time steps are executed.

11) Compare the vaporization time computed in step 9 with the input value in step 2. Update vaporization time as required and perform steps 3–10 again. This process converges rapidly in 2–3 iterations such that the vaporization time remains unchanged for subsequent iterations.

12) Generate results once the converged solution is obtained.

Typically, 500–1000 time steps are executed in a simulation. Grid function convergence studies have demonstrated that this resolution is sufficient to cause the solutions to be insensitive to the time step. The model was programmed in a MATLAB® script, and runtime is on the order of a few seconds on a current generation personal computer.[14]

Model Validation and Results

The model was validated against a series of experimental studies conducted at Purdue Univerity.[1,15] In these studies, 90% and 98% HP were injected downstream of a catalyst bed and the decomposition efficiency of the secondary injection was inferred from measured chamber pressures. Tests were conducted over a large range of secondary liquid injection percentages from 11 to 81% for chambers with characteristic lengths L^* ranging from 0.6223 to 1.384 m. The overall efficiency η_{tot} was determined from measured chamber pressure data and presumed to comprise a weighted average of the efficiency of the primary, η_{cat}, and secondary, η_s injectant efficiencies,

$$\eta_{\text{tot}} = r_s \eta_s + (1 - r_s)\eta_{\text{cat}} \tag{32}$$

where r_s is the ratio of secondary-to-primary (or secondary-to-catalyst bed) mass flows. When it is assumed that the catalyst bed is performing with perfect efficiency, $\eta_{\text{cat}} = 1$, the decomposition efficiency for the secondary stream was determined from measured chamber pressure.

The model was used to simulate this process inputting the theoretical catalyst bed conditions and using the measured chamber pressures. The model was run with the r_s value of interest, and the integration was concluded at the entry to the nozzle throat section. At this location, the η_{tot} value was assumed to be equivalent to the ratio of the unreacted HP vapor, m_{HP}, to the local mass of gas in the control volume, m. Equation (32) was then used to compute the corresponding η_s value. The droplet size was adjusted to match experimental data at $r_s = 0.2$, and the same drop size was then used for other r_s values to determine how well the model predicted the experimentally observed trends.

Figure 3 shows the experimental and analytical decomposition efficiencies for secondary injection of 90% peroxide. Here, the liquid mass fraction is the ratio of secondary mass flow to total mass flow, and this is plotted against the total percent of peroxide decomposition. A drop size of 100 μm, a reasonable value for a transverse jet injector as was used in the experiments, was assumed for all model simulations. Results show an excellent agreement over a wide range of liquid mass fraction values with the exception of the lone experimental data point at the very large flow split of 0.4. Figure 4 shows a similar comparison for the case where 98% fluid is used as the secondary injectant. Here, the best correlation with the more limited experimental results was obtained with a drop size of 135 μm. Because there is clearly a distribution of droplet sizes and the surface tension and density of the fluid do change somewhat from 90 to 98% concentration, there is good reason to expect that some adjustment in the drop size would be required in this case. Based on these encouraging results, the model was exercised over a broad range of conditions as summarized in the following section.

A baseline case was created to assess the detailed behavior of the secondary injection process. Values for model inputs for this case are summarized in Table 2. A modest 5% secondary injection was selected for study, and a typical catalyst bed flux of approximately 175.8 kg/s · m^2 was used in the simulations. Results from this case are shown in Figs. 5–8. In Fig. 5, the gas properties, nondimensionalized against their respective initial values, are plotted as a function of distance. The gas temperature drops initially due to the cooling effect

Table 2 Input parameters for baseline case

Parameter	Value	Units
Main catalyst bed flow HP concentration	90	%
Secondary liquid HP concentration	90	%
Main catalyst bed mass flow	0.091	kg/s
Secondary liquid mass flow (percent of main flow)	5	%
Chamber pressure	3,447,400	Pa
Chamber diameter	0.0254	m
Initial liquid HP drop diameter	100	μm
Initial liquid droplet temperature	317	K

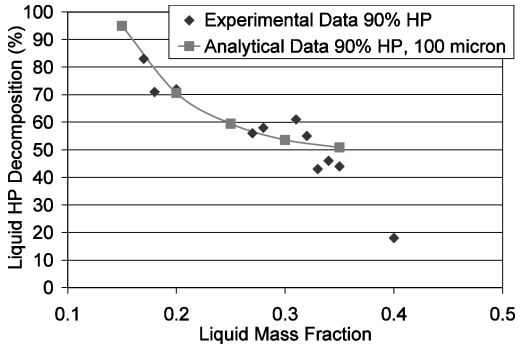

Fig. 3 Comparison of experimental decomposition efficiency measurements with model results for 90% HP secondary injection.[1]

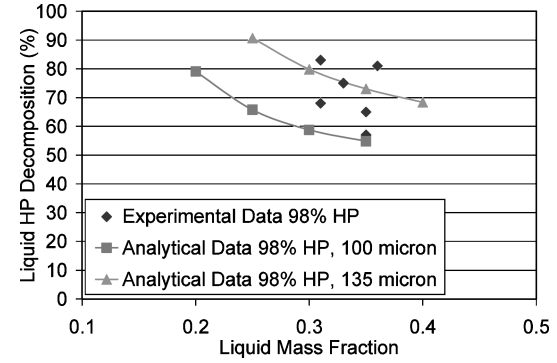

Fig. 4 Comparison of experimental decomposition efficiency measurements with model results for 98% HP secondary injection.[1]

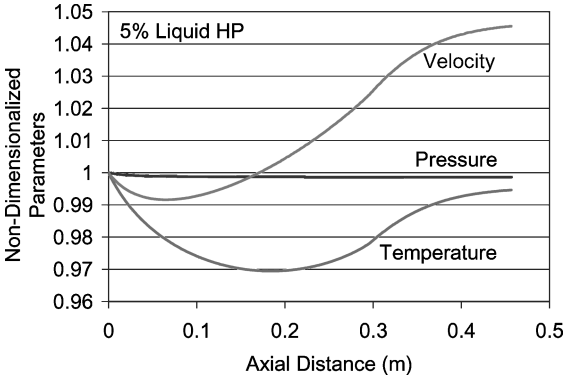

Fig. 5 Nondimensional pressure, temperature, and velocity for baseline case (Table 2) secondary injection conditions.

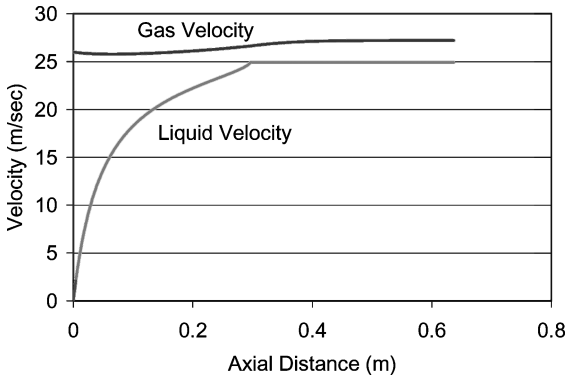

Fig. 6 Gas and liquid velocities for baseline case (Table 2) injection conditions.

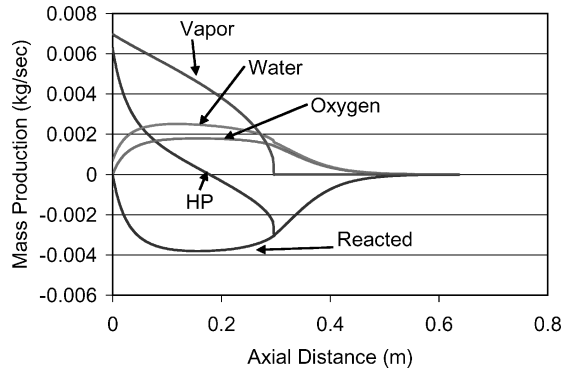

Fig. 7 Mass production rates for baseline case (Table 2) conditions.

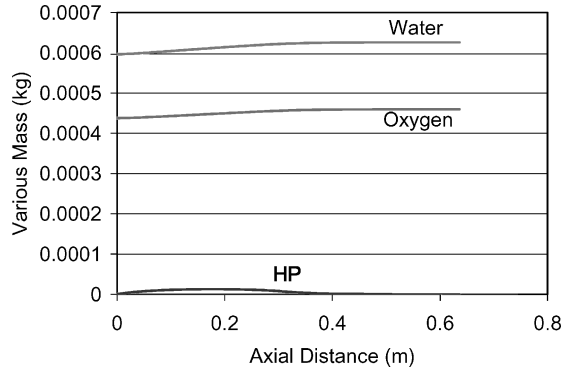

Fig. 8 Control volume masses for baseline case (Table 2) injection conditions.

of the droplet evaporation. As the thermal decomposition begins to occur, the temperature increases and asymptotically approaches the initial catalyst bed exhaust temperature. Because the model assumes negligible heat losses outside the system, the decomposition temperature should eventually be attained. Slight differences were observed in some cases due to the effects of variable specific heats used in the temperature integration. The minimum temperature attained in this baseline case corresponds to a 31 K decrease.

The pressure in the gas decreases very slightly for this modest injection condition because the gas must give up momentum to accelerate the drops to the local mixture velocity. The gas velocity has an interesting trend: The initial decrease is due to the cooling effect of the evaporation process raising the gas density in the control volume and thereby decelerating the flow. The increase in the latter stages is attributed to the additional mass represented by the evaporated drops. Probably the most compelling result of the simulation is the large axial distances required to achieve thermal decomposition for this baseline case of only 5% secondary injection.

Figure 6 shows a comparison of gas and liquid velocities for the baseline conditions. The drops are accelerated to a velocity very near that of the gas as they vanish at an axial distance of about 0.33 m from the injection point. Figure 7 shows the mass production rates for peroxide vapor, water, oxygen, and reacted fluid. Note that in this case the peak reaction rates occur roughly midway through the drop evaporation process. The droplet size has a strong effect on this behavior as will be noted in following parametric studies. Figure 8 shows the actual masses of the three constituents in the mixture showing a peak peroxide concentration in the region where the reaction rate is also a maximum (maximum negative value).

The baseline case results are depressing from the point that we are requiring 0.381–0.635 m of chamber length to permit the vaporization and thermal decomposition process to complete itself even for this modest 5% injection condition. To assess the reason for this unfortunate behavior, consider an isothermal case in which peroxide vapor is decomposed at various fixed gas temperatures. In this case, the reaction rate K is constant and an analytic solution exists for the concentration of HP as a function of time,

$$\ell n(C_{\mathrm{HP}}/C_{\mathrm{HP}\_0}) = -Kt$$

where C_{HP_0} is the initial concentration of HP vapor. We can define the half-life of this kinetic process, when $C_{\mathrm{HP}}/C_{\mathrm{HP}\_0} = \frac{1}{2}$ as

$$t_{\frac{1}{2}} = \ell n(2)/K$$

For the reaction activation energy and frequency factors provided in the kinetics model discussion, this half-life time is plotted as a function of temperature in Fig. 9. The right axis in Fig. 9 also shows the concentration of HP consistent with an adiabatic decomposition temperature on the left axis. Figure 9 provides some compelling results that point to the heart of the decomposition physics in this problem. For 90% HP, the decomposition temperature is around 1028 K, and the corresponding half-life time is roughly 1 ms. This implies that it takes about 1 ms to halve the concentration of HP vapor formed in a secondary injection process, a relatively long time given that gases traverse the combustion chamber in a comparable time interval. Of course, if substantial cooling results from the secondary injection, the process will take even longer because K drops exponentially with temperature.

Note the large sensitivity of the inherently exponential result. For temperature consistent with a 95% HP exhaust, the half-life time is decreased an order of magnitude to 0.1 ms. At bipropellant combustion temperatures, the decomposition process is literally measured on a microsecond timescale and is all but instantaneous in terms of the millisecond-level fluid mechanic-related times. Although a negative result in terms of a classical thermal decomposition, Fig. 9 points to the incredible benefits that can be obtained by conducting the thermal decomposition at higher temperatures. Prior experience with hybrid rockets running in the thermal decomposition mode have provided experimental confirmation of this result, that is, extremely efficient decomposition (and the subsequent combustion) can be attained in reasonable length combustion chambers.[16]

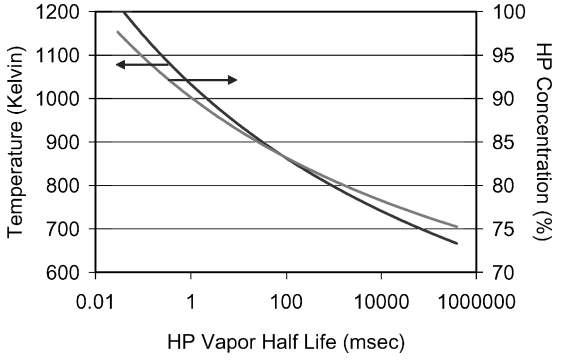

Fig. 9 Half-life decomposition time for HP vapor.

Parametric Studies

Although the prior results indicate great difficulties in achieving thermal decomposition of HP vapor in HP decomposition products, there is still much insight that can be obtained from conducting parametric studies with the model. Studies were conducted to assess independently the effects of varying the secondary liquid HP mass flow, the initial drop diameter, the secondary liquid HP concentration, the mass flux or gas velocity, and the droplet temperature, respectively. The following section provides a summary of these studies. Note that the percentage values indicated subsequently refer to a percentage of the primary (catalyst bed) flow being injected as the secondary flow.

Effect of Varying Secondary Liquid HP Mass Flow

The percentage of secondary liquid mass flow to main catalyst bed flow for 90% HP was varied to analyze the effect on the thermal decomposition process. All other input variables remained fixed at the values shown in Table 2. Figure 10 shows the resulting gas temperature distributions for various secondary liquid mass flow percentages of the main catalyst bed flow. The point where the curve ends represents the calculated decomposition distance. Note that, for the 14% injection case, the liquid injection nearly freezes the peroxide vapor concentration because the temperature drop is severe enough almost to eliminate the thermal decomposition mechanism. The reaction rate K drops from an initial value of over 600/s at the 1028 K temperature to 1.77/s at the 822 K minimum temperature of the evaporatively cooled gases. This dramatic reduction in reaction rate all but eliminates thermal decomposition.

Figures 11 and 12 present the effects of secondary injection level on gas pressures and velocities. Pressure drops increase with secondary injection because a larger amount of momentum exchange is required to accelerate the larger amounts of liquid, although overall drops in all cases are quite small. The drop in pressure in the latter stages of the process is due to Rayleigh losses associated with

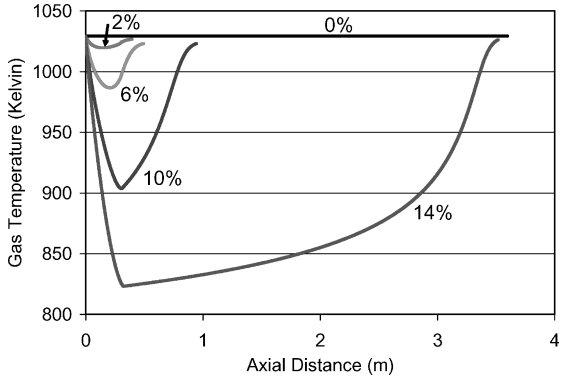

Fig. 10 Effect of percent secondary liquid injection on gas temperature, 90% HP.

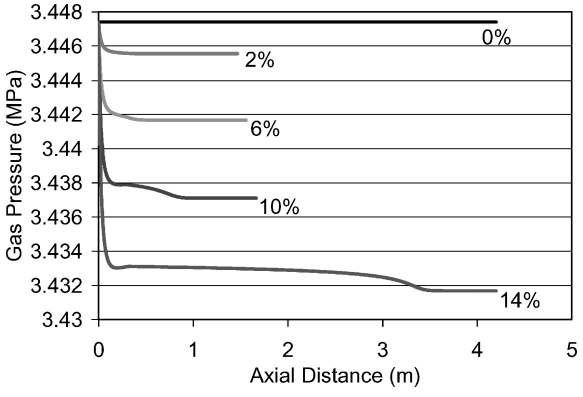

Fig. 11 Effect of percent secondary liquid injection on gas pressure, 90% HP.

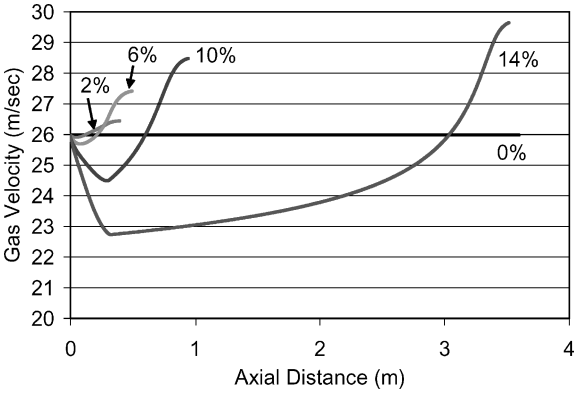

Fig. 12 Effect of percent secondary liquid injection on gas velocity, 90% HP.

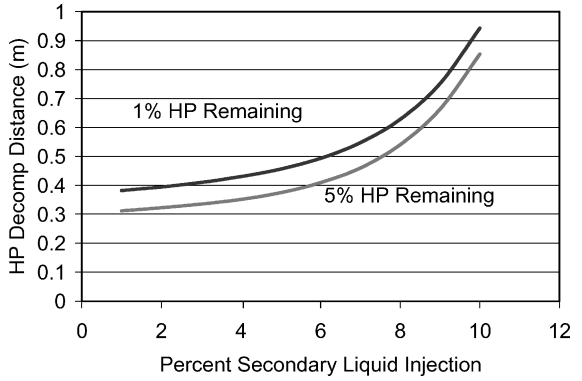

Fig. 13 Effect of percent secondary liquid injection on decomposition distance assuming 1 or 5% of original HP remains.

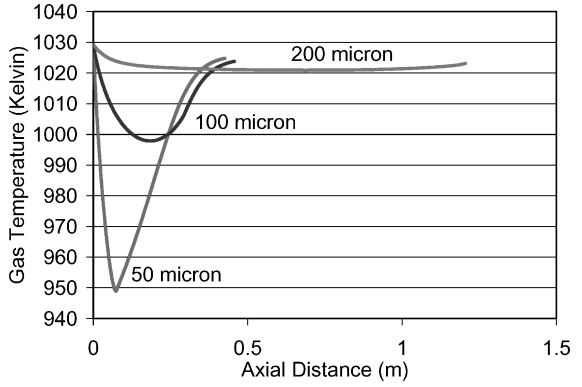

Fig. 14 Effect of initial droplet diameter on gas temperature, 50–200 μm.

the heat addition coming from the thermal decomposition process. Gas velocities increase according to the larger variations in flow attendant to larger liquid injection fractions. Figure 13 shows the decomposition distance as a function of percent secondary liquid injection assuming threshold values signaling the end of the process at 1 or 5% of the original peroxide present within the liquid. The results are disheartening in that large distances are required even for modest levels of secondary injection.

Effect of Initial Drop Diameter

The effect of initial drop diameter was explored for droplets ranging from 50 to 600 μm. All other inputs were maintained at the values provided in Table 2. The range of sizes considered gave very large ranges of decomposition distances; for this reason, results are summarized for smaller and larger drops in Figs. 14 and 15, respectively. For small drops, the process tends to be kinetics limited, that is, very

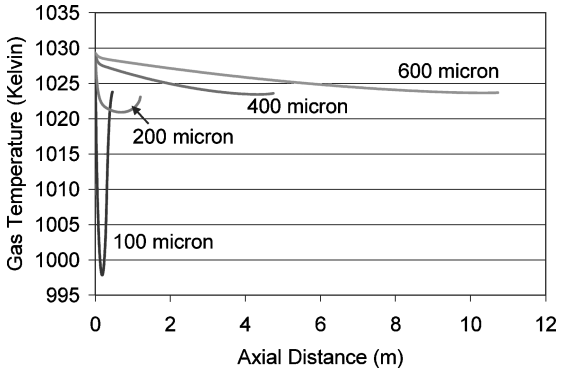

Fig. 15 Effect of initial droplet diameter on gas temperature, 100–600 μm.

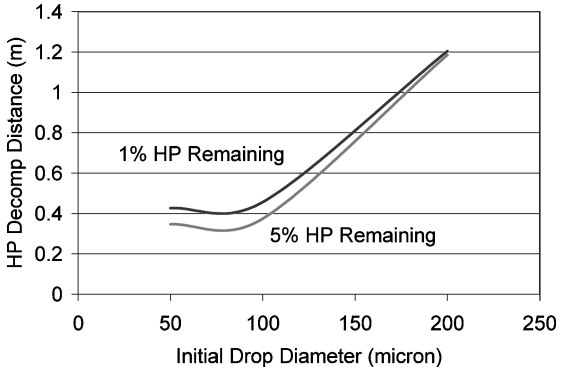

Fig. 16 Effect of initial droplet diameter on decomposition distance assuming 1 or 5% of original HP remains.

little decomposition occurs during the vaporization event due to its speed and the large amount of cooling occurring in this case. The larger drops show the opposite trend of being essentially vaporization limited in that the decomposition kinetics essentially keep the local vapor content very low as a result of the increased vaporization time. This result indicates some prospects of managing thermal decomposition processes using larger drops or lower evaporation rates. If a vertical structure can be created to enhance droplet lifetimes in a given chamber, then it may be possible to keep temperatures high enough to obtain efficient thermal decomposition. Figure 16 shows the resulting decomposition distances based on ending criteria of either 1 or 5% of the original peroxide present. Despite the deleterious effects of large evaporative cooling, the smaller drops still maintain shorter decomposition lengths than the larger drops for the configuration studied.

Effect of Secondary Liquid Hydrogen Peroxide Concentration

It was discovered that values of peroxide concentration below 90% produce unacceptably large decomposition distances in the cases already discussed. Whereas silver-based catalyst beds cannot operate using 98% fluid, it would be feasible to aft inject this fluid to increase energy content and promote more rapid decomposition. A study was conducted on this basis at various injection fractions with other input parameters fixed at values shown in Table 2. Figure 17 shows the effect of percent secondary liquid injection on gas temperature for various injection fractions. As in the 90% injection case (Fig. 10), the decomposition distance increases drastically when evaporative cooling drives gas temperatures below 840 K. Final temperatures exceed the initial values in this case due to the additional energy release in the decomposition of the 98% fluid. Figures 18 and 19 show the effect of gas pressure and velocity for 98% liquid peroxide with trends quite comparable to the 90% injection results. Figure 20 provides the resulting decomposition distances assuming 1 or 5% of the original peroxide remains, and Figure 21 shows a comparison of decomposition distances of 90 and 98%, assuming

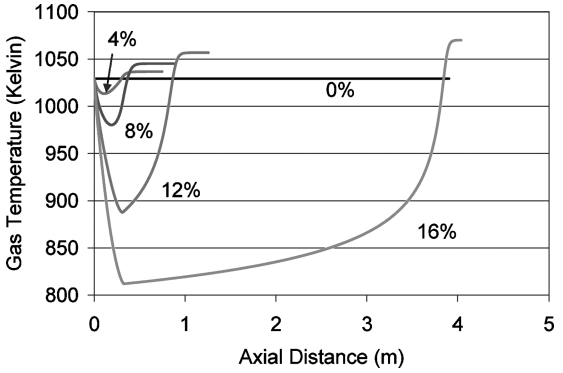

Fig. 17 Effect of percent secondary liquid injection on gas temperature, 98% HP.

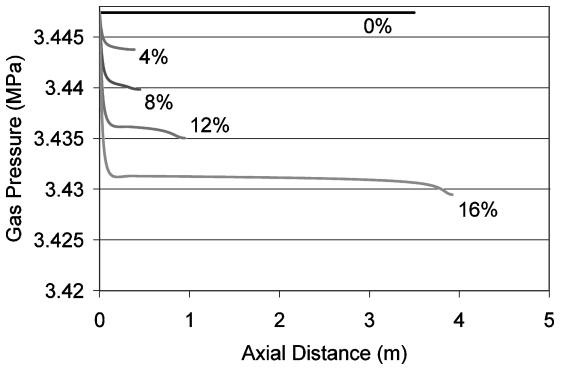

Fig. 18 Effect of percent secondary liquid injection on gas pressure, 98% HP.

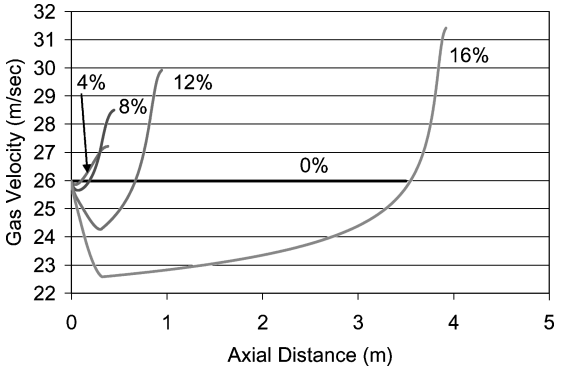

Fig. 19 Effect of percent secondary liquid injection on gas velocity, 98% HP.

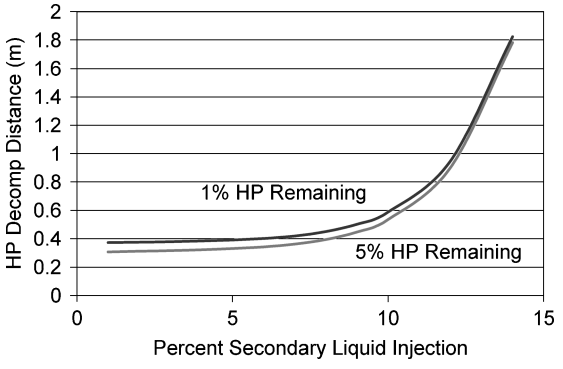

Fig. 20 Effect of 98% secondary liquid on decomposition distance assuming 1 or 5% of original HP remains.

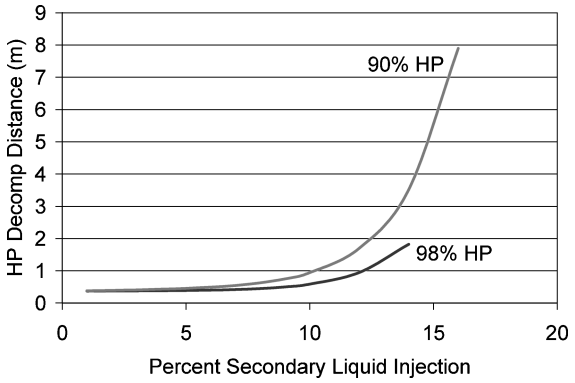

Fig. 21 Effect of 90 and 98% secondary liquid on decomposition distance assuming 1% of original HP remains.

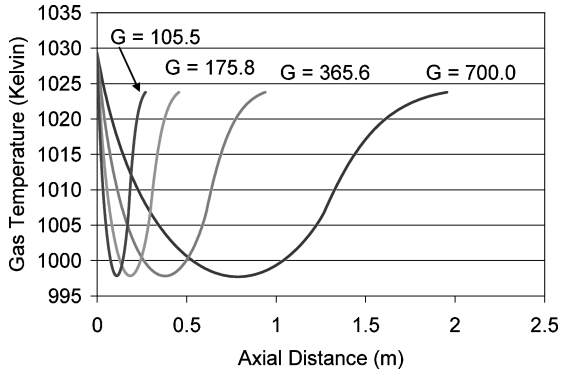

Fig. 22 Effect of mass flux (kilograms per square meter per second) on gas temperature, 90% HP.

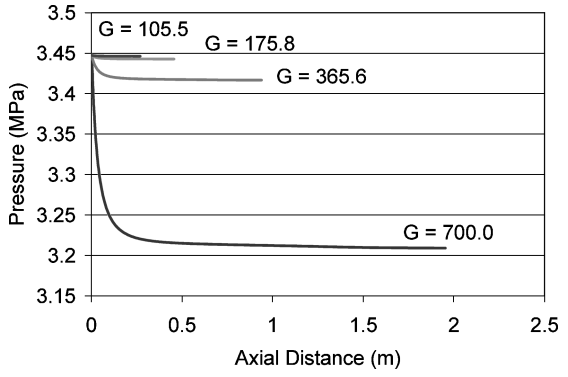

Fig. 23 Effect of mass flux (kilograms per square meter per second) on gas pressure, 90% HP.

1% of the original peroxide remains. Substantial benefits in the reduction of decomposition distance can be achieved using 98% fluid.

Effect of Catalyst Bed Mass Flux or Gas Velocity

The mass flux G was varied by changing the chamber diameter, which gave a mass flux range of approximately 105.5–700 kg/m^{2}s. Figures 22–24 show the resulting temperature, pressure, and velocity changes, respectively. Other inputs were maintained at the values shown in Table 2. Increasing mass flux basically increases gas velocity and stretches the axial coordinate accordingly. The higher velocities do create larger pressure drops (Fig. 23) because the momentum losses scale as ρv^2. The scaling of gas velocities with mass flux is shown in Fig. 24. The fact that increased mass flux essentially leads to a stretching of the axial distance, that is, events still occur over the same time interval, leads to a nearly linear relationship between decomposition distance and mass flux shown in Fig. 25.

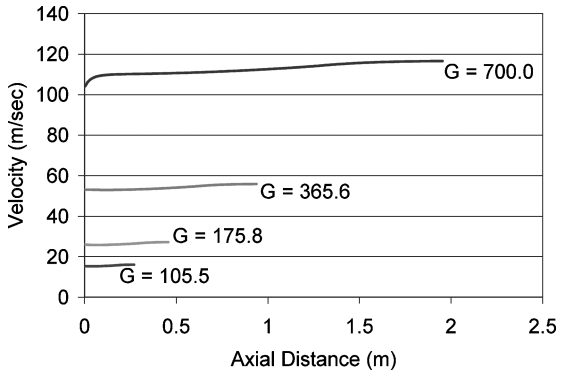

Fig. 24 Effect of mass flux (kilograms per square meter per second) on gas velocity, 90% HP.

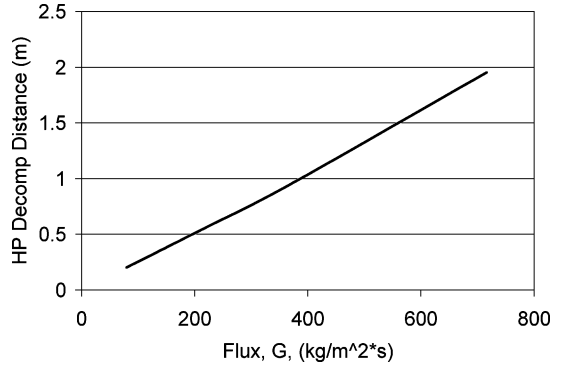

Fig. 25 Effect of mass flux (kilograms per square meter per second) on decomposition distance assuming 1% of original HP remains.

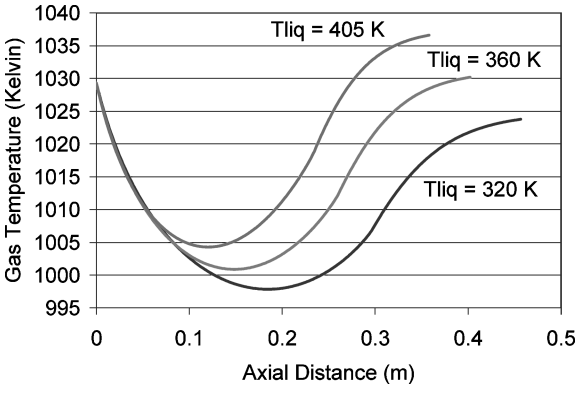

Fig. 26 Effect of droplet temperature on gas temperature, 90% HP.

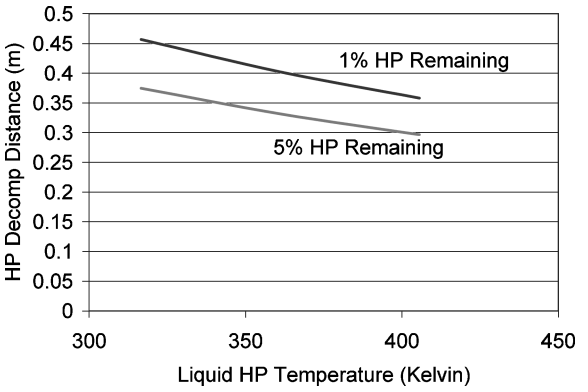

Fig. 27 Effect of droplet temperature on decomposition distance assuming 1 or 5% of original HP remains.

Effect of Injected Liquid Temperature

Some power cycles utilize the peroxide as a coolant before injection into the thrust chamber. For this reason, the effect of injectant temperature was investigated assuming remaining inputs remained at values shown in Table 2 with a 100-μm initial droplet diameter. Evaporation rates increase and gas subcooling effects decrease with increased liquid injectant temperature as noted in Fig. 26. The overall decomposition distance decreases accordingly as injectant temperature increases as shown in Fig. 27 for the 1% threshold indicating the decomposition length.

Conclusions

A one-dimensional model has been created to simulate the vapor-phase decomposition of HP in a gas stream composed of HP decomposition products. The tool includes the effects of the finite-rate vapor-phase kinetics, droplet evaporation and drag, and local gas temperature and pressure and can be used for arbitrary HP concentrations in both the main and secondary injectant streams. A single droplet size representative of the Sauter mean diameter of the parent spray is assumed in the integration. When this single parameter is adjusted within a range consistent for rocket injector sprays, excellent agreement is shown with measured data for the case of 90% HP injectant and main flows.[1]

A baseline case was selected to investigate 5% secondary injection of 90% HP into a 90% HP exhaust with a modest catalyst bed loading near 176 kg/m$^2 \cdot$ s. A 100-μm initial drop diameter was selected based on results from validation studies. The performance of the secondary injection for this case is disheartening in that reaction lengths on the order of 0.46 m are required even for this case of a fairly modest 5% secondary injection. The kinetic half-life of the vapor-phase decomposition process is computed to be on the order of milliseconds for temperatures consistent with 90% HP decomposition, but drops rapidly to microsecond levels at bipropellant combustion temperatures. This unfortunate condition limits the appeal of thermal decomposition for monopropellant applications, although at higher concentrations more reasonable reaction distances are obtained.

The amount of secondary injection had strong effects on decomposition distance because the evaporative cooling effect nearly quenches the thermal decomposition reaction at higher secondary injection rates. The initial droplet size also had profound effects on the decomposition process. For very small drops (less than 100 μm), the process is inherently kinetics controlled, with large amounts of evaporative cooling taking place before significant vapor-phase decomposition occurs. For large drops (greater than 200 μm), the process is inherently vaporization limited because the decomposition keeps up reasonably well with the evaporation rates. Even though the cooling effects lengthen the process, the smaller drops still had shorter decomposition lengths. There may be mechanisms to utilize larger drops and maintain gas temperature if novel strategies can be devised to increase chamber residence times.

Simulations were also conducted using 98% fluid as the secondary injectant. The increased energy of these drops did improve results somewhat, but reaction lengths were still too long to be of use in practical combustors for aerospace applications. Increasing the temperature of the injectant also had beneficial effects. Increasing the chamber velocities or catalyst bed mass fluxes essentially led to proportional increases in reaction lengths, that is, reaction times remained about the same.

Acknowledgments

This research was funded by a Phase I Small Business Technology Transfer awarded to IN Space, LLC, and Purdue University by the Missile Defense Agency (Contract F04611-03-M3207). Technical monitoring was provided by Alan Sutton of the U.S. Air Force Research Laboratory.

References

[1]Mok, J.-S., Helms, J., and Anderson, W., "Thermal Decomposition of Hydrogen Peroxide, Part 1: Experimental Studies," *Journal of Propulsion and Power*, Vol. 21, No. 5, 2005, pp. 942–953.

[2]Giguere, P. A., "The Thermal Decomposition of Hydrogen Peroxide Vapor II," *Canadian Journal of Research, Chemical Sciences*, Vol. 25, No. 2, 1947, pp. 135–150.

[3]Giguere, P. A., and Liu, I. D., "Kinetics of the Thermal Decomposition of Hydrogen Peroxide Vapor," *Canadian Journal of Chemistry*, Vol. 35, No. 4, 1957, pp. 283–293.

[4]Satterfield, C. N., and Stein, T. W., "Homogeneous Decomposition of Hydrogen Peroxide Vapor," *Journal of Physical Chemistry*, Vol. 61, No. 5, 1957, pp. 537–540.

[5]McLane, C. K., "Hydrogen Peroxide in the Thermal Hydrogen Oxygen Reaction I. Thermal Decomposition," *Journal of Chemical Physics*, Vol. 17, No. 4, 1949, pp. 379–385.

[6]Conway, D. C., "Mechanism of the Homogeneous Decomposition of Hydrogen Peroxide," *Journal of Physical Chemistry*, Vol. 61, No. 11, 1957, pp. 1579–1580.

[7]Hoare, D. E., Protheroe, J. B., and Walsh, A. D., "The Thermal Decomposition of Hydrogen Peroxide Vapour," *Transactions of the Faraday Society*, Vol. 55, 1959, pp. 548–557.

[8]Baldwin, R. R., and Brattan, D., "Homogeneous Gas-Phase Decomposition of Hydrogen Peroxide," *Proceedings of the Eighth International Symposium on Combustion*, Williams & Wilkins Co., 1962, New York, 1960, pp. 110–119.

[9]Hoffman, J. D., *Numerical Methods for Engineers and Scientists*, 2nd ed., Marcel Dekker, New York, 1992, pp. 364–370.

[10]Turns, S. R., *An Introduction to Combustion*, 2nd ed., McGraw–Hill, Boston, 1996, pp. 375, 376.

[11]Pearson, N., Pourpoint, T., and Anderson, W. E., "Vaporization and Decomposition of Hydrogen Peroxide Drops," AIAA Paper 2003-4642, July 2003.

[12]Shapiro, H. N., and Moran, M. J., *Fundamentals of Engineering Thermodynamics*, 3rd ed., Wiley, New York, 1996, pp. 219–262.

[13]*Hydrogen Peroxide Handbook*, Chemical and Materials Sciences Dept., Rocketdyne, AFRL-TR-67-144, Canoga Park, CA, July 1967, pp. 1–43.

[14]MATLAB, ver. 6.5, The Mathworks Inc., software program, Natick, MA, 2000.

[15]Mok, J.-S., Helms, J., and Anderson, W., "Decomposition and Vaporization Studies of Hydrogen Peroxide," AIAA Paper 2002-4028, July 2002.

[16]Wernimont, E. J., and Heister, S. D., "Combustion Experiments in a Hydrogen Peroxide/Polyethylene Hybrid Rocket with Catalytic Ignition," *Journal of Propulsion and Power*, Vol. 16, No. 2, 2000, pp. 318–326.